THE JOURNAL OF BIOLOGICAL CHEMISTRY VOL. 286, NO. 10, pp. 8597–8608, March 11, 2011

Molecular Basis of Wnt Activation via the DIX Domain Protein Ccd1*[S]

Received for publication, September 20, 2010, and in revised form, December 6, 2010 Published, JBC Papers in Press, December 28, 2010, DOI 10.1074/jbc.M110.186742

Yi-Tong Liu[‡], Qiong-Jie Dan[§], Jiawei Wang[‡], Yingang Feng[§], Lei Chen[‡], Juan Liang[‡], Qinxi Li[¶], Sheng-Cai Lin[¶], Zhi-Xin Wang[‡§], and Jia-Wei Wu[‡1]

From the [‡]MOE Key Laboratory of Bioinformatics, School of Life Sciences, Tsinghua University, Beijing 100084, China, the [§]Institute of Biophysics, Chinese Academy of Sciences, Beijing 100101, China, and the [¶]MOE Key Laboratory of Cell Biology and Tumor Cell Engineering, School of Life Sciences, Xiamen University, Xiamen, Fujian 361005, China

The Wnt signaling plays pivotal roles in embryogenesis and cancer, and the three DIX domain-containing proteins, Dvl, Axin, and Ccd1, play distinct roles in the initiation and regulation of canonical Wnt signaling. Overexpressed Dvl has a tendency to form large polymers in a cytoplasmic punctate pattern, whereas the biologically active Dvl in fact forms low molecular weight oligomers. The molecular basis for how the polymeric sizes of Dvl proteins are controlled upon Wnt signaling remains unclear. Here we show that Ccd1 up-regulates canonical Wnt signaling via acting synergistically with Dvl. We determined the crystal structures of wild type Ccd1-DIX and mutant Dvl1-DIX(Y17D), which pack into "head-to-tail" helical filaments. Structural analyses reveal two sites crucial for intra-filament homo- and hetero-interaction and a third site for inter-filament homo-assembly. Systematic mutagenesis studies identified critical residues from all three sites required for Dvl homo-oligomerization, puncta formation, and stimulation of Wnt signaling. Remarkably, Ccd1 forms a hetero-complex with Dvl through the "head" of Dvl-DIX and the "tail" of Ccd1-DIX, depolymerizes Dvl homo-assembly, and thereby controls the size of Dvl polymer. These data together suggest a molecular mechanism for Ccd1-mediated Wnt activation in that Ccd1 converts latent polymeric Dvl to a biologically active oligomer(s).

Wnt signaling is one of the major developmental pathways regulating various cellular processes (1–3). In the canonical pathway, the extracellular Wnt ligands regulate the expression of specific target genes by modulating the amount of β-catenin. In the absence of Wnt, degradation of β-catenin is mediated by a destruction complex containing adenomatous polyposis coli, glycogen synthase kinase-3β, casein kinase I, and Axin.[2] Binding of Wnt ligands to the Frizzled and low density lipoprotein receptor-related protein 5 and 6 (LRP5/6) receptors results in the activation of Dishevelled (Dvl), which suppresses β-catenin degradation. Thus, β-catenin is accumulated in the cytosol and subsequently translocated into the nucleus to regulate Wnt target genes.

Dvl and Axin contain a conserved region of about 100 residues, referred to as the DIX domain (4). The cytoplasmic Dvl has a tendency to form puncta via its DIX domain (Dvl-DIX), which may mediate Wnt signaling by reversible polymerization to provide an interaction platform for other Wnt components, including Axin (5–9). The DIX domain of Axin (Axin-DIX) is also required for the formation of Axin polymers and puncta (10, 11). Proper intracellular transduction of Wnt signal relies on the direct interaction between Dvl and Axin (11, 12). It is generally believed that the DIX domains play important roles in the formation of Dvl-Axin complex, although isolated Dvl-DIX and Axin-DIX do not bind to each other directly either *in vivo* or *in vitro* (9, 11–13). In addition to Dvl and Axin, the coiled-coil protein DIX domain-containing 1 (Ccd1) also contains a DIX domain that can form heteromeric complexes with Dvl and Axin and, thus, positively regulate the canonical Wnt signaling (14). Ccd1 is highly conserved in species ranging from zebrafish to human and is shown to play important roles in neurogenesis, axonal morphogenesis, and neuronal migration (15–18).

The x-ray structure of Axin-DIX was determined and revealed a helical filament in crystal and led to a head-to-tail self-association model of the DIX domain (5). However, the DIX domain of Axin cannot form hetero-complexes with either Dvl-DIX or Ccd1-DIX and is dispensable for the canonical Wnt signaling. In contrast, both DIX domains of Ccd1 and Dvl are indispensable for their hetero-interaction and the regulation of Wnt signaling. Therefore, the homomeric interaction revealed in the crystal packing of Axin-DIX might not fully define the nature for the interactions between the DIX domains. To reveal the molecular basis, we determined the crystal structures of wild type Ccd1-DIX and mutant Dvl1-DIX(Y17D) and carried out extensive biochemical studies on how the DIX domain-containing proteins can dynamically modulate each other. Despite their monomeric nature, these

* This work was supported in part by Ministry of Science and Technology of China Grants 2007CB914400 and 2011CB910803, National Natural Science Foundation of China Grant 31070643, and Tsinghua University Grant 09THZ02235.

[S] The on-line version of this article (available at http://www.jbc.org) contains supplemental Figs. 1–4.

The atomic coordinates and structure factors (codes 3PZ7 and 3PZ8) have been deposited in the Protein Data Bank, Research Collaboratory for Structural Bioinformatics, Rutgers University, New Brunswick, NJ (http://www.rcsb.org/).

[1] To whom correspondence should be addressed. Tel.: 86-10-62789387; Fax: 86-10-62792826; E-mail: jiaweiwu@mail.tsinghua.edu.cn.

[2] The abbreviations used are: Axin, axis inhibition protein; Dvl, Dishevelled; DIX, Dishevelled and Axin; Ccd1, coiled-coil-DIX1; HSQC, heteronuclear single quantum coherence.

two DIX domains are engaged in similar homo-oligomeric contacts, forming helical filaments in crystals. Structural analyses and systematic mutagenesis studies revealed that the critical residues for the DIX-DIX interaction are from three sites, two intra-filament sites (Site I and Site II) and one inter-filament site (Site III). The integrity of all three sites is required for Dvl homo-assembly, puncta formation, and Wnt signal transduction, whereas the non-conservative Site II in Axin-DIX may account for its disability to form hetero-complex with Dvl-DIX and Ccd1-DIX. In addition, we found that Ccd1 regulates Wnt signaling via association with Dvl through the head of Dvl-DIX and the tail of Ccd1-DIX. Importantly, Ccd1 depolymerizes the homo-assembly of Dvl *in vitro* and induces its diffuse cytoplasmic distribution *in vivo*. Our data together with prior work disclose the activation mechanism of Ccd1 by directly interacting with Dvl, depolymerizing the high molecular weight Dvl homopolymer, and further stabilizing Dvl in its biologically active low molecular weight state.

EXPERIMENTAL PROCEDURES

Constructs, Mutagenesis, and Protein Purification—The DIX domains of human Ccd1 (residues 386–472), mouse Dvl1 (3–104), and mouse Dvl2 (10–122) were amplified by standard PCR procedures and inserted into pET21b or pGEX2T vectors with a C-terminal His_6 tag or N-terminal GST tag. Point mutations in DIX domain were generated by overlap PCR procedures and subjected to DNA sequencing. All proteins, overexpressed in *Escherichia coli* BL21(DE3) cells at 20 °C were first purified over nickel-nitrilotriacetic acid (Qiagen) or glutathione-Sepharose (GE Healthcare) columns and then by ion exchange (Source-15Q/15S, GE Healthcare) followed by gel filtration chromatography (Superdex-200, GE Healthcare) at 4 °C. The proteins were stored at −80 °C and subject to crystallization trials or biochemical assays.

Crystallization, Data Collection, and Structure Determination—Crystals of Ccd1-DIX were grown using the hanging drop vapor diffusion method by mixing Ccd1-DIX protein (~10 mg/ml) with an equal volume of reservoir solution containing 0.1 M sodium cacodylate, pH 6.5, 0.3 M magnesium nitrate, 15% PEG 3350, and 4% DMSO at 4 °C. The diffraction data sets were collected at the Beijing Synchrotron Radiation Facility (Beijing, China) to a resolution of 3.0 Å. Unfortunately, the molecular replacement was unsuccessful. To solve the phase problem, we introduced a mutation of L436M to enhance the selenomethionine signal. Rod clusters of the selenomethionine-substituted protein (~8 mg/ml) were observed with a reservoir containing 0.1 M sodium cacodylate, pH 6.5, 20% PEG 3350, 4% ethylene glycol, and 0.2 M ammonium acetate. Single crystals were obtained by micro-seeding at 4 °C and grew to full size after 1 week. The crystals were cryoprotected in the reservoir solution supplemented with 20% glycerol and flash-frozen under cold nitrogen stream at 100 K. The diffraction data were collected to 2.44 Å at the selenium edge (0.97904 Å) at beamline NW12 at Photon Factory (Tsukuba, Japan) with an ADSC CCD detector. The crystals belong to space group $P6_122$, with $a = b = 62.4$ Å, $c = 77.7$ Å, $\alpha = \beta = 90°$, $\gamma = 120°$, and comprise one molecule per asymmetric unit. Data were processed by the HKL-2000 package (19). The structures were successfully solved by the single-wavelength anomalous dispersion phasing method using SHELXD (20). Standard refinement was performed with the programs REFMAC (21) and Coot (22). The final model of Ccd1-DIX was refined to the *R* and free *R* values of 23.3 and 27.3%.

Crystals of Dvl1-DIX(Y17D) (~10 mg/ml) appeared after 2–3 days and grew to full size after 1 week with a reservoir solution containing 0.1 M Hepes, pH 7.2, 10% ethylene glycol, 0.66 M sodium citrate, and 0.3 M sodium chloride at 22 °C. The crystal was dehydrated in 1.0 M sodium citrate for 40 min and flash-frozen without additional cryoprotectant. The diffraction data sets for Dvl1-DIX(Y17D) were collected to 2.85 Å at beamline 17U1 at the Shanghai Synchrotron Radiation Facility and processed using the HKL-2000 package (19). The crystals belong to space group $I2_12_12_1$, with $a = 92.7$ Å, $b = 106.8$ Å, $c = 266.0$ Å, $\alpha = \beta = \gamma = 90°$, and comprise eight molecules per asymmetric unit. The structure was solved by molecular replacement using Phaser using Ccd1-DIX as the search model (23). Standard refinement was performed with the programs Phenix (24) and Coot (22). The final model of Dvl1-DIX(Y17D) was refined to the *R* and free *R* values of 23.1% and 26.1%.

The data processing and refinement statistics are summarized in Table 1. All structural representations in this paper were prepared with PyMOL. The atomic coordinates and structure factors have been deposited with the Protein Data Bank under accession codes 3PZ7 for Ccd1-DIX and 3PZ8 for Dvl1-DIX(Y17D).

Gel Filtration Analysis—Size exclusion chromatography using a Superdex 200 10/300 column on an ÄKTA FPLC (GE Healthcare) was carried out to assess the apparent molecular weight of a protein in solution and the interaction between two proteins at 4 °C. The column was equilibrated with a buffer containing 10 mM Tris-HCl, pH 8.0, 150 mM NaCl, and 2 mM dithiothreitol (DTT) at a flow rate of 0.5 ml/min. All protein samples or mixtures were diluted with the equilibration buffer to indicated concentrations and incubated at 4 °C for 30 min. Each sample at a volume of 500 μl was loaded to the column, and fractions of 0.5 ml each were collected. Aliquots of relevant fractions were subjected to SDS-PAGE, and proteins were visualized by Coomassie Blue staining. The column was calibrated with molecular mass standards.

GST-mediated Pulldown Assay for Protein-Protein Interaction—~0.4 mg of recombinant GST-tagged protein A was bound to 0.2 ml of glutathione-Sepharose 4B resin pre-equilibrated with a buffer containing 25 mM Tris-HCl, pH 8.0, 150 mM NaCl, and 2 mM DTT. To remove excess unbound protein A or other contaminants, the resin was washed 5 times with 0.5 ml of buffer. Then 0.6 mg of non-tagged protein B was allowed to flow through the resin. After extensive washing, the bound proteins were eluted with 5 mM reduced glutathione and visualized by SDS-PAGE with Coomassie Blue staining.

Analytical Ultracentrifugation—The Dvl2-DIX and Ccd1-DIX proteins were purified and concentrated to ~2 mg/ml in a buffer containing 10 mM Tris and 150 mM NaCl. The sam-

ples for analytical ultracentrifugation analyses contain 0.8 mg/ml Dvl-DIX and/or 0.5 mg/ml Ccd1-DIX proteins as indicated. Sedimentation velocity experiments were conducted at 20 °C using a Beckman ProteomeLab XL-A ultracentrifuge with an An60 Ti rotor. After an initial scan at 3,000 rpm to check the total absorbance, sedimentation runs were performed at 42,000 rpm with scans continuously collected at a 3-min interval. The sedimentation profiles were analyzed using the continuous distribution ($c(s)$) analysis module in the program Sedfit Version 11.0 (25).

NMR Spectroscopy—Ccd1 were uniformly labeled with ^{13}C,^{15}N by growing the recombinant strain in M9-minimal medium containing $^{15}NH_4Cl$ and [^{13}C]glucose as the sole nitrogen and carbon sources, respectively. The labeled proteins were purified as described above. Samples for NMR measurements contained 0.5 mM Ccd1-DIX in 50 mM potassium phosphate, pH 7.0, 90% H_2O, 10% D_2O, and 0.01% sodium 2,2-dimethylsilapentane-5-sulfonate (DSS). All NMR experiments were carried out at 310 K on a Bruker DMX 600 MHz spectrometer with a triple resonance cryo-probe. NMR experiments for ^1H, ^{15}N, and ^{13}C backbone resonance assignments included ^1H-^{15}N HSQC, ^1H-^{13}C HSQC, three-dimensional HNCACB, CBCA (CO) NH, HNCO, HN (CA) CO, HBHA (CBCA), and CONH. All NMR spectra were processed and analyzed using Felix software (Accelrys, Inc.). Proton chemical shifts and ^{15}N and ^{13}C chemical shifts were referenced to internal sodium 2,2-dimethylsilapentane-5-sulfonate (DSS) and indirectly to DSS, respectively.

Plasmids, Cell Culture, and Transfection—pCDNA-HA-Dvl2, pEGFP-C3-Dvl2, and pCMV5-Myc-Ccd1 were generated according to standard molecular techniques. Mutation and deletion/truncation constructs were generated by overlap PCR strategy. The authenticities of all constructs were confirmed by nucleotide sequencing. HEK293T and Simian COS7 cells were maintained in DMEM medium (Invitrogen) supplemented with 10% fetal bovine serum, 100 μg/ml penicillin, and 100 μg/ml streptomycin (Sigma). Transfection was performed using Lipofectamine^{TM} 2000 (Invitrogen) according to the manufacturer's instructions.

Luciferase Reporter Assay—The Wnt activities of Dvl and Ccd1 (wild type or mutants) were examined with the luciferase assay. HEK293T cells were seeded into 96-well plates, and the indicated amounts of plasmids were transfected with 15 ng of Wnt reporter SuperTOPFlash that contained 8 copies of T-cell factor binding sites upstream of the luciferase coding sequence. The plasmid pRL-TK (0.5 ng) served as an internal control. At 36 h after transfection, cells were lysed, and luciferase assays were carried out with the Dual-Luciferase reporter assay system (Promega). Activation of Wnt signaling was quantified by measuring relative firefly luciferase activity normalized to Renilla luciferase.

RNA Interference—The 19-mer oligonucleotides specific for human Ccd1 (5′-GGATGCCTTGCAGCAGAG-3′) was inserted into the pSUPER vector as reported (26). The expression of Ccd1 was analyzed by immunoblotting using anti-Myc antibody. GFP was used as a control for transfection efficiency. To knock down human Dvl2 and Dvl3, siRNAs against Dvl2 and Dvl3 were designed and synthesized according to previous report (27). Briefly, HEK293T cells were pretreated with a 100 nM mixture of Dvl2/3 siRNAs or non-targeting control siRNAs. After 24 h of culture, cells were transfected with indicated expressing vectors, and the luciferase reporter assays were carried out at 36 h after transfection.

Immunofluorescence Analysis—To examine the puncta formation, simian COS7 cells were cultured on glass coverslips in 6-well plates and transfected each with 1 μg of DNA of HA-tagged Dvl wild type or mutants. At 24 h after transfection, cells were fixed with 4% paraformaldehyde for 20 min, permeabilized with 0.2% Triton X-100 for 10 min, and then blocked with 5% BSA for 1 h. The staining was performed by anti-HA antibodies and followed by secondary antibodies conjugated with Alexa Fluor 568 (Molecular Probes, Invitrogen). The localization of HA-Dvl was then visualized on a fluorescence microscope. For colocalization analysis, COS7 cells were co-transfected with 0.5 μg of GFP-Dvl and 0.5 μg of Myc-Ccd1. Fixation of cells was carried out similarly at 24 h post-transfection. Dvl localization was visualized by the intrinsic fluorescence of GFP, whereas Ccd1 proteins were revealed by indirect immunofluorescence using anti-Myc antibodies and Alexa Fluor 568-conjugated rabbit anti-mouse secondary antibodies. Stained cells were examined using a confocal microscope.

RESULTS

Ccd1 Activates Wnt Signaling through Dvl—Ccd1 was identified as a positive regulator in canonical Wnt signaling. We examined the Wnt signaling activity of Ccd1 using the β-catenin-responsive reporter SuperTOPFlash that contains eight copies of T-cell factor/Lymphoid Enhancing Factor binding sites upstream to the luciferase gene. Ectopically expressed Ccd1 resulted in Wnt activation, which was comparable to the activation induced by over-expressing Dvl (14, 28). To further assess the importance of Ccd1, we knocked down the endogenous Ccd1 by transfecting HEK293T cells with shRNA specific for Ccd1. When pSUPER-Ccd1 was cotransfected with Wnt3a, the Wnt3a-mediated transcriptional activation was strongly suppressed to ~30% of the original activation (Fig. 1*A*). These results demonstrate that Ccd1 indeed plays a role in the activation of Wnt signaling.

Because Ccd1 can interact with Dvl, we asked whether Ccd1 functions through Dvl. To address this issue, we depleted endogenous Dvl in HEK293T cells by RNAi and assessed the effect on Wnt activation by ectopically expressed Ccd1. In higher organisms (including mammals), there are three Dvl isoforms, Dvl1, Dvl2 and Dvl3, and they were reported to function similarly and cooperatively in positively mediating the canonical signaling (29–34). The abundance of endogenous Dvl1 was extremely low whereas Dvl2 and Dvl3 constituted over 99% of the total pool in HEK293 cells, and a mixture of Dvl2/3 siRNAs was thus used to knockdown endogenous Dvl proteins (27, 35). As shown in Fig. 1*B*, depletion of Dvl significantly down-regulated Wnt3a-mediated activation. Similarly, the stimulation of Wnt signaling by Ccd1 was substantially suppressed, indicating that Dvl is required for Ccd1-mediated Wnt activation. Remarkably, coexpression of Ccd1 and Dvl dramatically stimulated the T-cell factor/

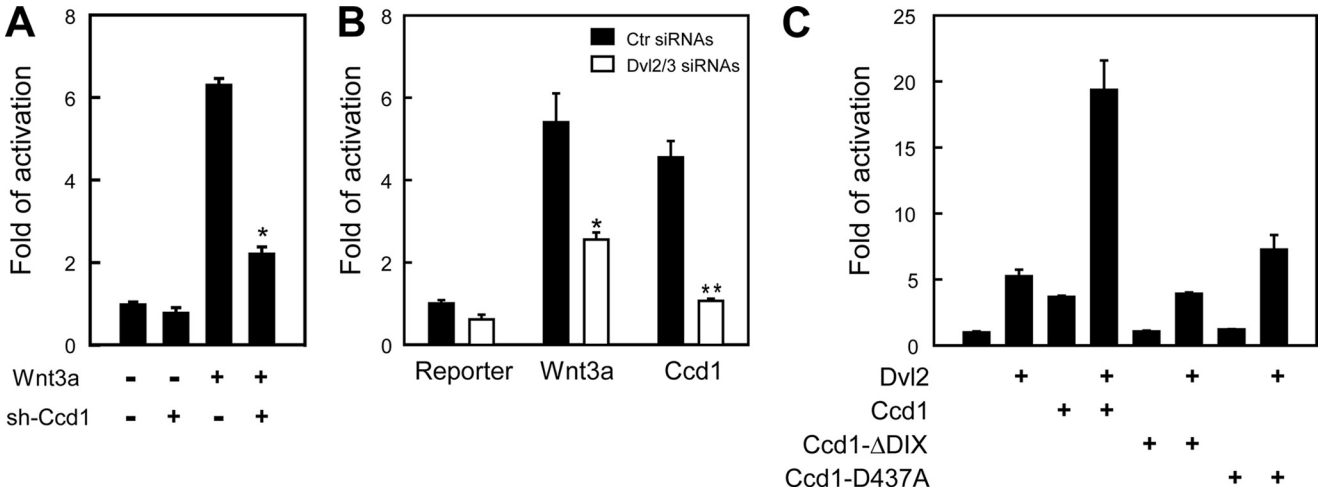

FIGURE 1. **Ccd1 activates canonical Wnt pathway through Dvl.** *A*, knockdown of endogenous Ccd1 attenuates Wnt-3a mediated T-cell factor transcriptional activity. HEK293T cells were transfected with Wnt-3a (0 or 2 ng) and pSUPER-Ccd1 (0 or 30 ng) as indicated. Some 36 h later the activation of Wnt signaling was quantified by luciferase activity. *Asterisks* denote $p < 0.001$ when compared with the corresponding samples only transfected with Wnt-3a. *B*, knockdown of endogenous Dvl suppresses Ccd1 function. HEK293T cells were cotransfected with 100 nM Dvl2/3 siRNAs together with Wnt-3a (2 ng) or Ccd1 (10 ng). *, $p < 0.05$; **, $p < 0.005$ compared with the corresponding samples transfected with control siRNAs. *Ctr*, control. *C*, synergistic effects of Dvl and Ccd1 on Wnt activation. Some 10 ng of Myc-Ccd1 (wild type or truncation/mutations as indicated) were transfected into HEK293T cells with or without Dvl2 (10 ng).

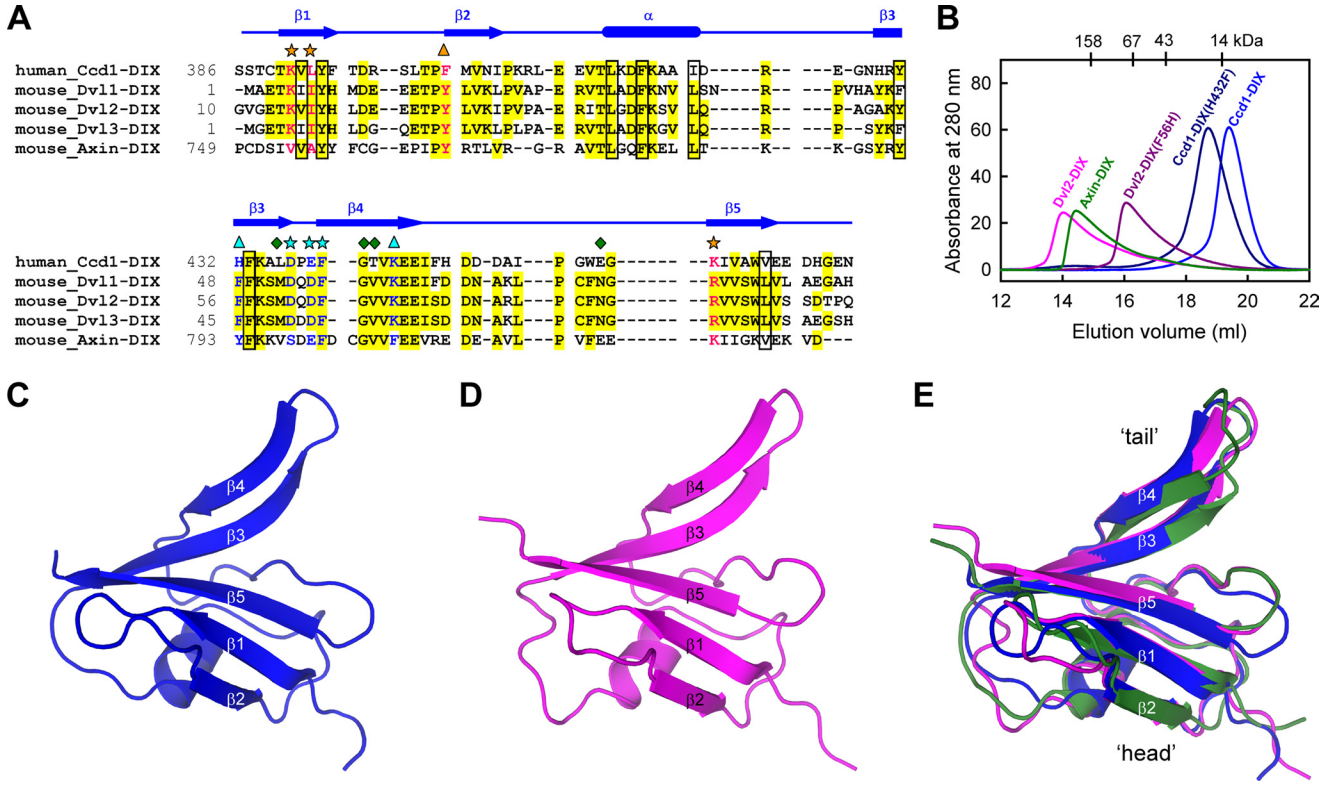

FIGURE 2. **Crystal structures of Ccd1-DIX and Dvl1-DIX(Y17D).** *A*, sequence alignment of the DIX domains from human Ccd1, mouse Dvl1–3, and mouse Axin. Secondary structural elements of Ccd1-DIX are indicated in *blue*, and the hydrophobic core residues are *boxed*. Residues at Site I and Site II are indicated, respectively, by *triangles* and *asterisks*, and residues at the head and tail of the DIX domain are colored, respectively, by *orange* and *cyan*. Residues at Site III are indicated by *green diamonds*. *B*, oligomerization states of Dvl-DIX, Axin-DIX, Ccd1-DIX, and their swap mutants are shown. The size exclusion chromatography was performed to determine the apparent molecular weight of the DIX domains/mutants at a concentration of ~50 μM. *C* and *D*, schematic representations of Ccd1-DIX and Dvl1-DIX(Y17D) are shown. Both structures adopt the ubiquitin-like fold, and the β-strands are labeled. *E*, superposition of three DIX structures, Ccd1-DIX (*blue*), Dvl1-DIX(Y17D) (*magenta*), and Axin-DIX (*green*, PDB code 1WSP). The head and tail essential for DIX-DIX interaction are also indicated.

Lymphoid Enhancing Factor-mediated transcription, whereas Ccd1 or Dvl alone yielded a modest activation of the reporter (Fig. 1*C*). Therefore, these data demonstrated that Ccd1 and Dvl synergistically stimulate Wnt signaling.

Crystal Structure of Ccd1-DIX—Ccd1 directly interacts with Dvl via their DIX domains, and we, thus, cloned and purified these DIX domains (Fig. 2*A*). A notable property of Dvl and Axin is their ability to form via their conserved DIX do-

TABLE 1
Data collection and refinement statistics

	Ccd1-DIX	Dvl1-DIX(Y17D)
Data collection[a]		
Space group	$P6_122$	$I2_12_12_1$
Cell dimensions		
a, *b*, *c* (Å)	62.4, 62.4, 77.7	92.7, 106.8, 266.0
α, β, γ (°)	90, 90, 120	90, 90, 90
Resolution (Å)	50.0-2.44 (2.53-2.44)[b]	50.0-2.85 (2.95-2.85)
R_{merge} (%)	11.0 (60.8)	5.3 (66.1)
$I/\sigma(I)$	18.6 (2.6)	23.1 (2.1)
Completeness (%)	99.9 (100.0)	99.8 (100.0)
Redundancy	5.8 (5.4)	3.7 (3.8)
Wilson B-value (Å^2)	42.6	85.3
Refinement		
Resolution (Å)	31.58-2.44 (2.53-2.44)	41.0-2.85 (2.95-2.85)
No. reflections	3,680	30,176
R_{work}/R_{free}	23.3/27.3	23.1/26.1
No. atoms		
Protein	751	5,376
Water	40	41
B-factors		
Protein	40.2	88.7
Water	42.4	90.0
R.m.s. deviations		
Bond lengths (Å)	0.012	0.009
Bond angles (°)	1.48	1.20
Ramachandran angles		
Most favored	65 (85.5%)	468 (80.6%)
Additionally allowed	9 (11.8%)	108 (18.6%)
Generously allowed	2 (2.6%)	5 (0.9%)
Disallowed	0 (0.0%)	0 (0.0%)

[a] Both data sets were collected from single crystal.
[b] The highest resolution shell is shown in parentheses.

mains large protein assemblies. Consistently, recombinant Dvl2-DIX and Axin-DIX were eluted similarly as homopolymers in the gel filtration analysis (Fig. 2*B*). However, the retention time of Ccd1-DIX corresponded to an apparent molecular mass of 11 kDa, in reasonable agreement with its calculated monomeric molecular mass of 10 kDa. The oligomerization states of Dvl2-DIX and Ccd1-DIX were also characterized by analytical ultracentrifugation (see Fig. 7*B*). The sedimentation coefficient of the polymeric Dvl2-DIX was determined to be 4.7 S, comparable with previous result (5), whereas that of Ccd1-DIX was 1.5 S, consistent with its monomeric nature. To elucidate the molecular mechanism of DIX domain in Wnt signaling, we carried out crystallization trials for Ccd1-DIX and Dvl-DIX. Unfortunately, thus far all attempts to crystallize the wild type DIX domains of all three Dvl isoforms have been unsuccessful, likely due to heterogeneity of the large Dvl assemblies.

We solved the crystal structure of Ccd1-DIX by single wavelength anomalous dispersion (Table 1). Ccd1-DIX was composed of one five-stranded β-sheet ($\beta1$-$\beta5$) and one short α-helix, characteristic of the β-grasp (ubiquitin-like) fold (Fig. 2*C*). The amphipathic α-helix packs against the concave face of the mixed β-sheet, involving hydrophobic residues that are highly conserved among all DIX domains and other structurally related proteins (supplemental Fig. S1). All of these residues are invariant or highly conserved throughout three DIX domain-containing proteins and other structurally related proteins (Fig. 2*A*). The structure of Ccd1-DIX is readily superimposable to the previously determined structure of Axin-DIX (5) with an overall root mean square deviation of 1.6 Å over 80 core C_α atoms. The major structural deviations were mapped to the loop regions (Fig. 2*E*). In particular, the subtle conformational change of the $\beta3$-$\beta4$ loop is critical to the interactions between these DIX domains (see below).

Determinant for the Monomeric Nature of Ccd1-DIX—Consistent with the polymeric state in solution, Axin-DIX was found to engage in homomeric head-to-tail interactions in crystals (5). Interestingly, inspection of crystal packing in the structure of Ccd1-DIX revealed the presence of a similar helical filament (Fig. 3*A*), although this crystallographically derived model may not be physiologically relevant. In the crystallographic dimers of both Axin-DIX and Ccd1-DIX, the head (strands $\beta1$ and $\beta2$ and the C terminus of α-helix) of Molecule A interacts with the tail (strands $\beta3$ and $\beta4$) of the adjacent Molecule B. The protein-protein interfaces are centered at the intermolecular backbone hydrogen bonds between strand $\beta2$ of Molecule A and strand $\beta4$ of Molecule B that run approximately perpendicular to each other.

This intermolecular interaction involves two potential sites. As shown in Fig. 3*D*, there is a cluster of hydrophobic residues on the Axin-DIX interface composed of Tyr 766 from strand $\beta2$ of Molecule A and Tyr-793 and Phe-807 from strands $\beta3$ and $\beta4$ of Molecule B (5). These residues are conserved in Dvl-DIX (Fig. 2*A*), and the side chains of the corresponding Tyr-27, Phe-56, and Lys-68 of Dvl2 likely preserve this hydrophobic patch as the methylene group of Lys would provide the hydrophobic contact as well. However, the hydrophobic Tyr/Phe is replaced by a polar residue His-432 in Ccd1-DIX (Fig. 3*B*), which may account for its monomeric nature. To assess this structure-based hypothesis, we individually swapped the residues of Ccd1-DIX or Dvl2-DIX with the corresponding amino acids and analyzed their oligomeric states in solution by gel filtration (Fig. 2*B*). Indeed, mutating His-432 of Ccd1-DIX into hydrophobic Phe led to an increase of the elution volume, suggestive of a change in the oligomer-monomer equilibrium. In turn, when Phe-56 of Dvl2 was replaced by histidine, the mutant protein formed low molecular weight oligomers compared with the wild type Dvl2. As expected, the conserved substitutions, mutation of Phe on strand $\beta2$ to Tyr or vice versa, had no impact on the oligomerization states of Ccd1-DIX and Dvl2-DIX (data not shown). These data clearly indicate that this hydrophobic interface plays an important role in the homomeric DIX-DIX interactions of Dvl assemblies and that the presence of a basic residue histidine leads to the monomeric nature of Ccd1-DIX.

Additional Contacts in DIX-DIX Self-association of Dvl—Further analysis of the crystal packing of Ccd1-DIX has enabled us to identify additional contacts between each two adjacent molecules (Fig. 3*C*). Phe-440 from the heavily twisted $\beta4$-strand at the tail of Molecule B inserts into a hydrophobic pocket on the head of Molecule A, lined by aliphatic side chains of Leu-393 and the hydrophobic methylene groups of Lys-391 and Lys-460. In addition, the positively charged Lys-391 on head strand $\beta1$ interacts with two acidic amino acids, Asp-437 and Glu-439, from the tail $\beta3$-$\beta4$ loop. Sequence alignment between Ccd1 and Dvl reveals a high degree of conservation within the residues that comprise this binding site (Fig. 2*A*), suggesting an augmentative role of this region in the formation of Dvl homo-assemblies and the hetero-interaction between Dvl and Ccd1. However, Axin-

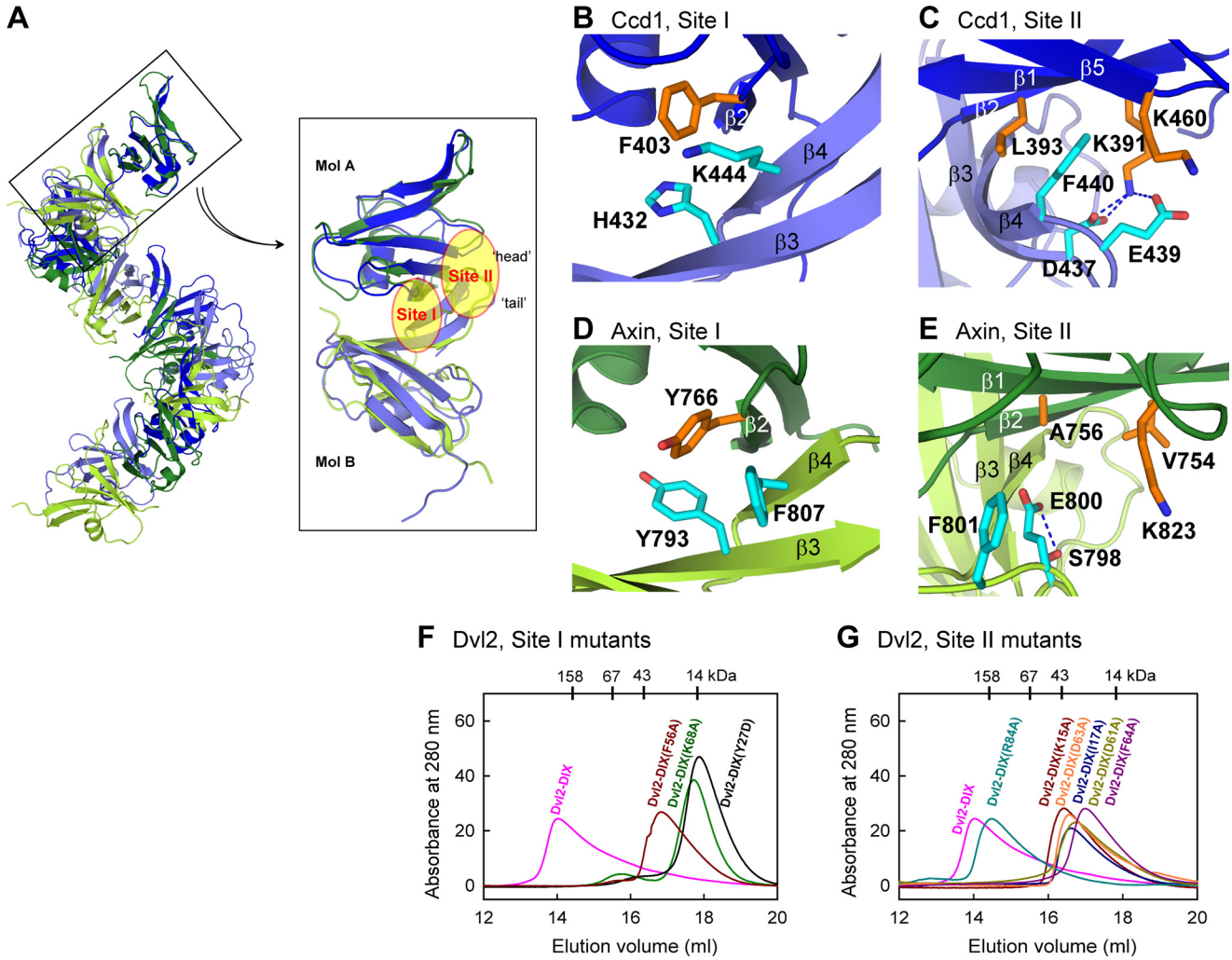

FIGURE 3. **Crystal structure of Ccd1-DIX reveals additional contacts for head-to-tail DIX-DIX interaction.** *A*, helical filaments in crystals of Ccd1-DIX (*blue* and *slate*) and Axin-DIX (*green* and *lemon*) are shown. The top molecule of each filament is superimposed. Site I and Site II that mediate the head-to-tail interactions are indicated on the superposed hetero-dimers on the *right*. *B–E*, close-up views of Site I and Site II at the interfaces of Ccd1-DIX and Axin-DIX heterodimers. The molecules are colored the same as in *panel A*, and critical residues from the head and tail are highlighted in *orange* and *cyan*, respectively. *F* and *G*, oligomerization states of Dvl2-DIX Site I and Site II mutants determined by gel filtration analyses. The protein concentration used was approximate 50 μM.

DIX does not seem to possess an interactive conformation in Site II, as the corresponding Phe-801 in Axin shifts outwards more than 6 Å (Fig. 3*E*). For simplicity, the previously defined hydrophobic patch essential for Dvl and Axin homopolymerization is hereafter referred to as Site I, and the new patch as Site II.

Schwarz-Romond *et al.* (5) have proposed a model for Dvl2-DIX oligomer based on the Axin-DIX filament structure, which demonstrated the importance of the hydrophobic Site I in mediating Dvl homo-oligomerization. To verify the importance of the new Site II on Dvl self-assembly, we generated a series of point mutations on Dvl2-DIX and examined their effect on its polymerization. Remarkably, the Site I mutations, Y27D at the head and K68A at the tail, led to two monomers, and mutant F56A was eluted as the low molecular weight oligomer (Fig. 3*F*). When the corresponding interface residues at Site II were individually mutated, most of the Dvl2-DIX mutants were markedly retained on the size exclusion column, indicating a dissociation of Dvl polymer (Fig. 3*G*). In the analytical ultracentrifugation analyses, the sedimentation coefficient of the monomeric Site I mutant Y27D was approximately 1.7 S and that of wild type Dvl2-DIX was ~4.7 S as reported (5). Notably, the Site II mutant F64A showed an intermediate sedimentation value of 2.4 S, confirming that this mutant exhibits impaired polymerization ability (supplemental Fig. S2). Together, these results indicated that Site I indeed plays a significant role in Dvl homo-assembly, and Site II exerts an auxiliary function.

Crystal Structure of Dvl1-DIX(Y17D)—Because the crystallization trials for wild type Dvl-DIX were unsuccessful, we turned to solve the structure of Dvl-DIX mutants to validate the Dvl homopolymerization model. We successfully generated diffractable crystals of a Dvl-DIX mutant, *i.e.* Dvl1-DIX(Y17D) containing residues 3–104, and solved the structure by molecular replacement using Ccd1-DIX as searching model (Table 1). The structure of Dvl1-DIX(Y17D) has essentially the same topology as the other two DIX domains, and the C-terminal tail (residues 84–104) is disordered (Fig. 2*D*

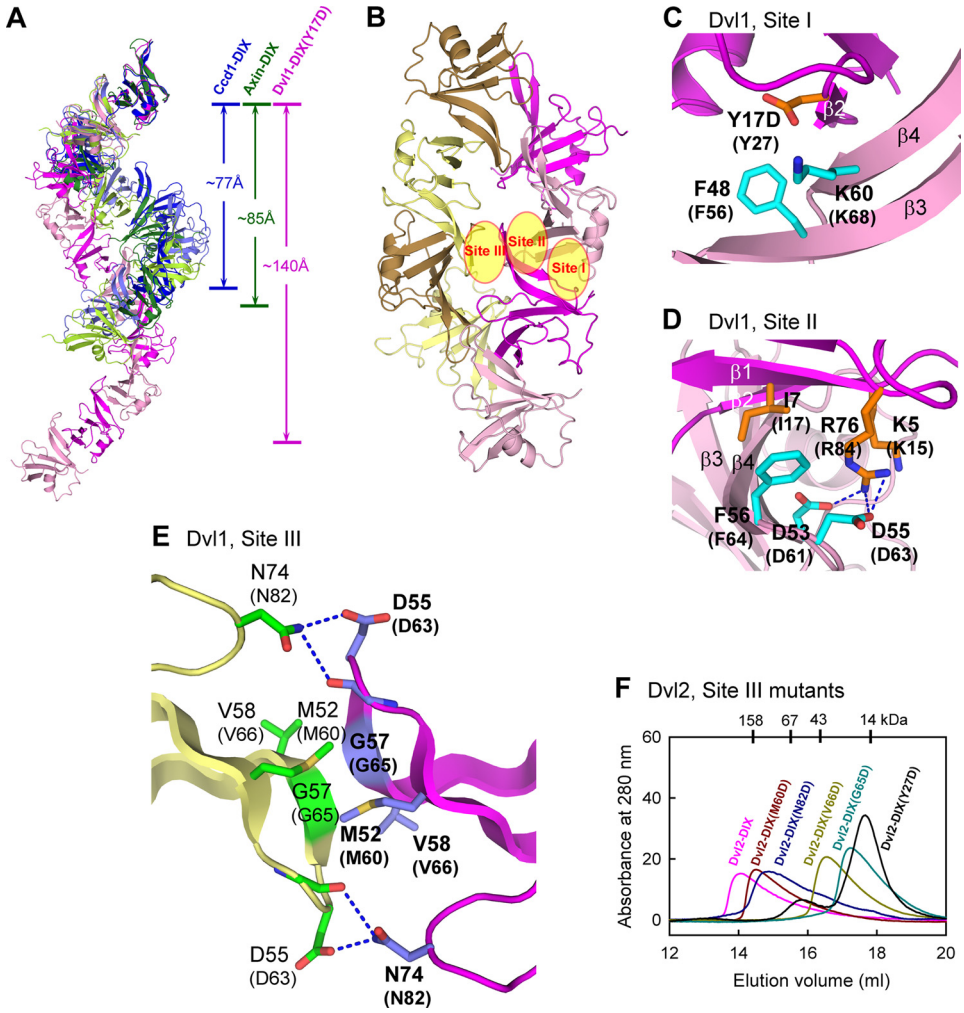

FIGURE 4. **Crystal structure of Dvl1-DIX(Y17D) indicates interfilament contacts crucial for Dvl polymerization.** *A*, different arrangements of the helical filaments in crystals of Ccd1-DIX (*blue* and *slate*), Dvl1-DIX(Y17D) (*magenta* and *pink*), and Axin-DIX (*green* and *lemon*) are shown. The top molecule of each filament is superimposed, and the helical pitches of three filaments are indicated. *B*, eight Dvl1-DIX(Y17D) molecules within an asymmetric unit packed into two intertwined helical filaments. The molecules forming two filaments are colored in *magenta*/*pink* and *sand*/*yellow*, respectively. Three sites for Dvl homopolymerization are indicated. *C* and *D*, close-up views of Site I and Site II at the intrafilament interface of Dvl1-DIX(Y17D) are shown. The orientations are the same as in Fig. 3, *B* and *C*, respectively. Residues from the head and tail are highlighted in *orange* and *cyan*, respectively, and corresponding Dvl2 residues are labeled in *parentheses*. *E*, close-up view of Site III at the interfilament interface of Dvl1-DIX(Y17D). Residues from two adjacent molecules are highlighted in *green* and *slate sticks*. *F*, oligomerization states of Dvl2-DIX Site III mutants (~50 μM) are characterized by gel filtration analyses. The profiles for wild type Dvl2-DIX and mutant Y27D were also shown for comparison.

and supplemental Fig. S1). Because of the introduction of a charged side chain into the hydrophobic interface, mutant Dvl1-DIX(Y17D) was a monomer in solution regardless of the protein concentration (supplemental Fig. S3); however, it packs into a head-to-tail polymer in the crystal (Fig. 4*A*). The arrangements of the crystallographic helical filaments of 3 DIX domains are slightly different; Ccd1-DIX, like Axin-DIX, assembles into a compact helical structure of 6 molecules per turn and with a pitch of approximately 80 Å, whereas Dvl1-DIX(Y17D) packs into a loose polymer with 8 molecules per turn and a pitch of ~140 Å.

Intriguingly, the eight Dvl1-DIX(Y17D) molecules within an asymmetric unit polymerize into a pair of intertwined right-handed helical filaments (Fig. 4*B*). A close-up view of the crystallographically intermolecular interface reveals that Dvl possesses the hydrophobic patch as in Axin despite the Y17D mutation (Fig. 4*C*). Notably, the intermolecular Site II newly identified in Ccd1-DIX is highly conserved in the crystallographic assembly of Dvl1-DIX(Y17D), reaffirming its role in DIX-DIX interaction (Fig. 4*D*). Further inspection of the crystal packing of Dvl1-DIX revealed that a novel symmetric interface (hereafter referred to as Site III) between two adjacent molecules form distinct filaments in addition to the two intra-filament sites (Fig. 4*E*). Met-52 and Val-58 from the β3-β4 hairpins of Dvl1 make hydrophobic contacts to the equivalent residues on the adjacent molecule. Notably, two glycine residues (Gly-57) are positioned closely at the center of this hydrophobic interface. The polar side chain of Asn-74 from the loop N terminus to strand β5 of one molecule hydrogen bonds to the side-chain carboxyl group of Asp-55 and the carbonyl oxygen of Gln-54 on the β3-β4 loop of the adjacent molecule. This interface is largely conserved in Axin-DIX, but the Thr substitution on strand β4 of Ccd1-DIX is likely to disturb the hydrophobic contacts (Fig. 2*A*). To investigate the importance of this site, corresponding mutants of Dvl2-DIX were generated, and their abilities to form olig-

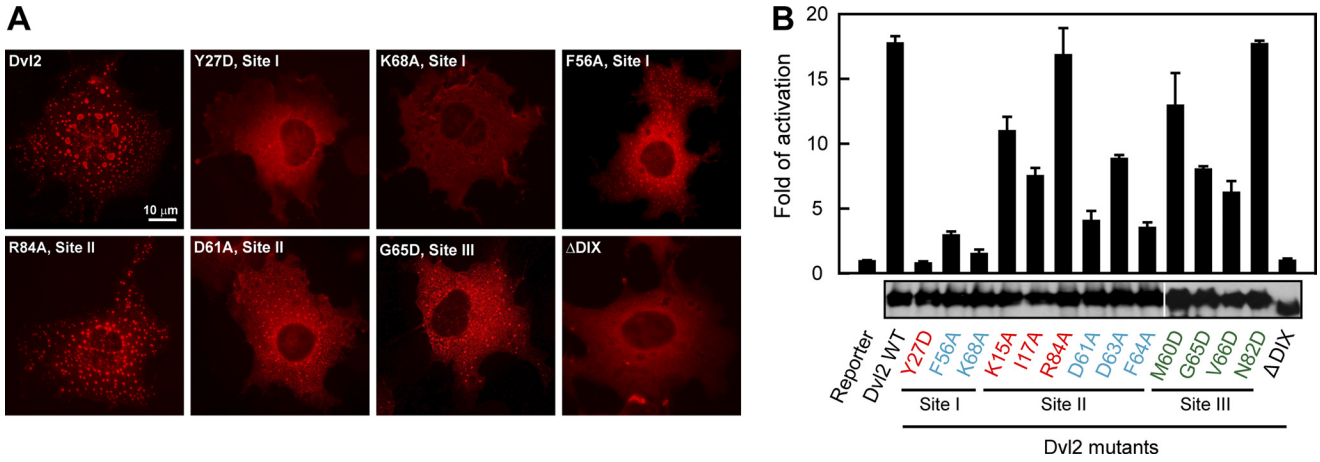

FIGURE 5. **Oligomerization via DIX domain is required for Dvl puncta formation and Wnt stimulation.** *A*, puncta formation of full-length Dvl2 wild type and representative mutants is shown. COS7 cells were transfected with 1 μg of HA-tagged Dvl2, and the localization of Dvl2 was visualized by indirect immunofluorescence. *Scale bar*, 10 μm. *B*, Wnt activities of full-length Dvl2 wild type and mutants. Some 20 ng of HA-Dvl2 mutants were transfected into HEK293T, and TOPFLASH reporter assays were performed to determine the Wnt activities after 36 h. The *bottom panel* shows the expression levels of all Dvl2 mutants detected by Western blotting using anti-HA antibodies.

omers were examined by gel filtration and velocity ultracentrifugation analyses. As shown in Fig. 4*F*, mutant V66D formed low molecular weight oligomers, whereas mutation of Asn-82 or Met-60 to Asp exhibited little effect on Dvl polymerization. Moreover, substitution of Gly-65 with any other amino acid would introduce steric clashes into the tightly packed inter-filament Site III, and mutant G65D was, thus, defective in polymerization (Fig. 4*F* and supplemental Fig. S2*D*). These data suggested that, in addition to the filament formation via Sites I and II, Dvl may further assemble into higher-order aggregates via Site III.

DIX-DIX Assembly of Dvl Is Important for Puncta Formation and Wnt Signaling—Because the polymerization of Dvl is believed to be crucial for its physiological function, we next examined the effect of these mutations in full-length Dvl2 on puncta formation and Wnt signaling. As shown in Fig. 5*A*, mutant R84A of Dvl2 that retains the ability of polymerization gave rise to puncta formation in a pattern indistinguishable from that of wild type Dvl2. However, mutants Y27D and K68A that behaved as monomers *in vitro* as well as the DIX domain truncation (Dvl2-ΔDIX, residues 95–736) were evenly distributed in the cytoplasm of transfected simian COS7 cells. Interestingly, mutants F56A, D61A, and G65D from three distinct sites, which only polymerized into low molecular weight oligomers, formed somewhat smeared puncta, indicating that these mutants possess a modest tendency to polymerize at high concentrations. Remarkably, the ability of these mutants to stimulate Wnt signaling, assessed by using TOPFlash reporter, correlated precisely with their respective ability of self-association and puncta formation (Fig. 5*B*). That is, ectopic expression of wild type Dvl2 and mutant R84A each led to a stimulation of the Wnt reporter by greater than 15-fold. In contrast, the monomeric mutants (Y27D and K68A) diffused in cytosol were completely defective in signaling as that observed for the DIX truncation mutant (ΔDIX). Partial activations were detected for mutants with impaired ability of self-assembly and puncta formation. Thus, these results strongly suggested that Dvl homopolymerization via its DIX domain is a critical process during the initiation of Wnt signaling.

Heteromeric Interaction between the Head of Dvl-DIX and the Tail of Ccd1-DIX—To elucidate the molecular mechanism underlying how Ccd1 regulates the intracellular Wnt signal transduction through hetero-interaction with Dvl, we first examined this hetero-interaction using purified Dvl2-DIX and Ccd1-DIX. When Ccd1-DIX was applied to GST-Dvl2-DIX preimmobilized to glutathione resin (Fig. 6*A*, *first lane*) or vice versa (Fig. 6*C*, *first lane*), these two DIX domains formed a stable hetero-complex as resolved by SDS-PAGE. In view of the high sequence similarity, structure homology, and similar crystal packing mode, we hypothesized that Dvl-DIX and Ccd1-DIX form a hetero-complex in a similar head-to-tail pattern.

To investigate the exact interface on Ccd1-DIX, we performed NMR titration studies. The addition of non-labeled Dvl2-DIX into ^{15}N-labeled Ccd1-DIX resulted in changes of the peaks in the ^{1}H-^{15}N HSQC spectra, and peak disappearance was observed due to the size increase or slower exchange rate of the protein complex at the NMR timescale (supplemental Fig. S4). Residues displaying significant peak intensity changes were mostly clustered on strands β3 and β4, the tail of Ccd1-DIX, distributing over both sites (Fig. 6*D*). To complement the NMR analysis, we carried out systematic GST-mediated pulldown assays. Some of the Ccd1-DIX mutants, K444A on Site I and D437A and F440A on Site II, abolished the formation of Ccd1-Dvl2 hetero-complex, indicating that both Sites I and II of Ccd1 are required for its interaction with Dvl (Fig. 6*A*). The NMR data also suggested the involvement of the β1-β2 loop, but mutation of those indicated residues had little effect on *in vitro* binding analysis (data not shown). Notably, all three effective mutations are located at the tail of Ccd1-DIX, whereas none of the head mutants disrupted the hetero-assembly (Fig. 6*D*). Next, we generated various mutations in the backbone of full-length Ccd1 and determined their effects using the Wnt reporter assay. Consistent with their affinities to Dvl, the tail mutants D437A, F440A, and

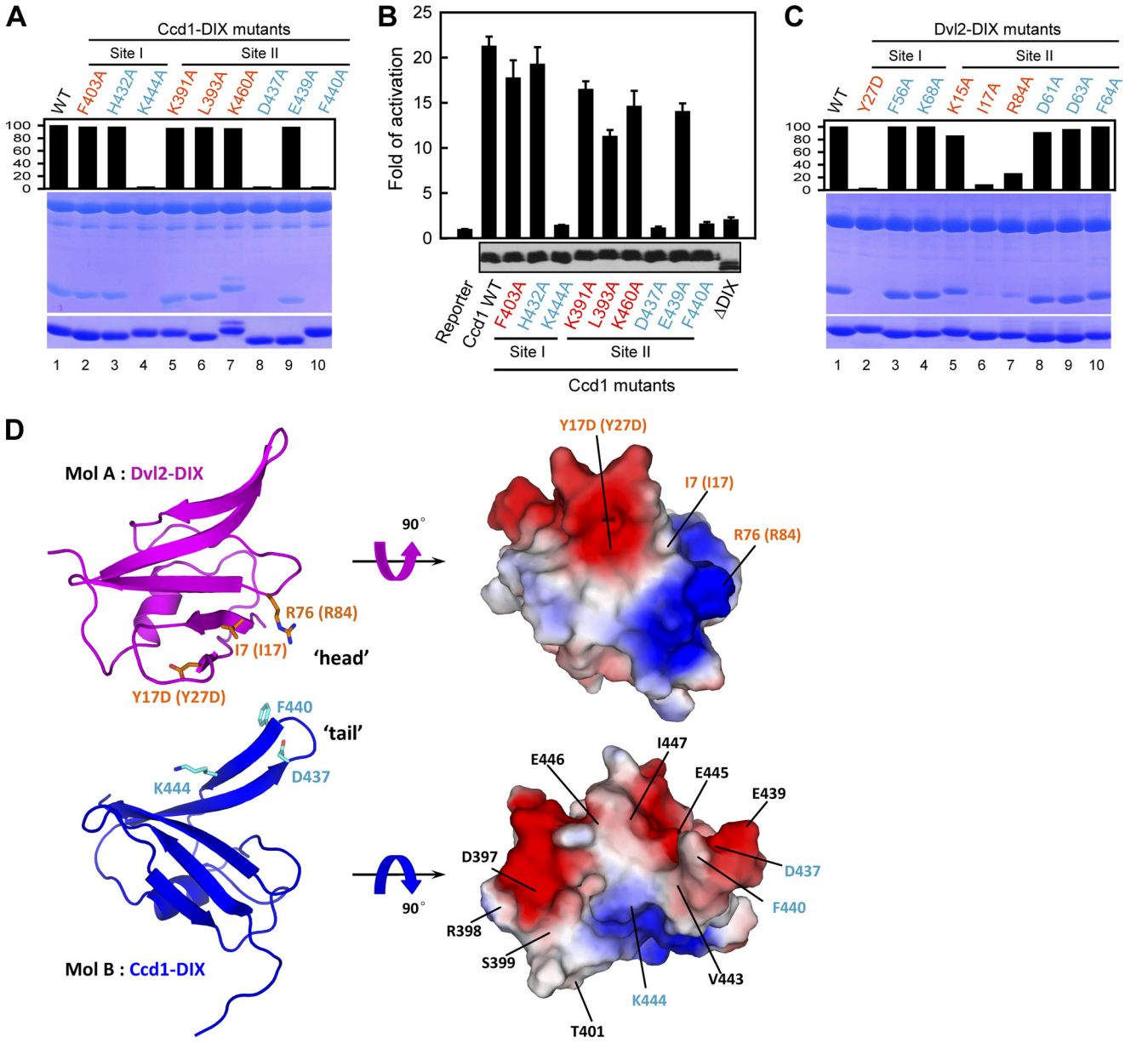

FIGURE 6. **Hetero-interaction between head of Dvl-DIX and tail of Ccd1-DIX.** *A*, determination of Dvl2-binding sites on Ccd1-DIX is shown. Glutathione beads immobilized with wild type GST-Dvl2-DIX were used to pull down Ccd1-DIX mutants. The *top panel* shows the relative affinities of Ccd1 mutants to Dvl2, with the affinity of wild type Ccd1 defined as 100%. The *middle panel* is the electrophoretic pattern of Dvl2-DIX and Ccd1-DIX after GST pulldown assays. The protein amounts of Ccd1-DIX mutants used are shown at the *bottom*. *B*, Wnt signal activities of Ccd1 mutants correlate precisely with their abilities to interact with Dvl. TOPFLASH reporter assays were performed to determine the Wnt activities of full-length Myc-Ccd1 mutants. The expression levels of all Ccd1 mutants detected by Western blotting using anti-Myc antibodies are shown at the *bottom*. *C*, shown is identification of Dvl2 residues required for Ccd1 interaction. The GST-mediated pulldown assays were carried out with GST-tagged wild type Ccd1-DIX and various Dvl2-DIX mutants. The panels are arranged the same as in *A*. *D*, schematic and surface representations of the hetero-interaction between Dvl2-DIX (*magenta*) and Ccd1-DIX (*blue*) are shown. The two surface representations, colored according to electrostatic potential (positive, *blue*; negative, *red*), are oriented by a 90° rotation around a *horizontal axis* as indicated, respectively. The key interface residues at the head of Dvl2-DIX and the tail of Ccd1-DIX are, respectively, highlighted in *orange* and *cyan*, and those Ccd1 residues displaying significant chemical shift changes in NMR titration are labeled in *black*.

K444A as well as the DIX domain truncation mutant (ΔDIX) were unable to activate the Wnt reporter, whereas mutants that retain the heteromeric interaction with Dvl mostly reserved the ability of Wnt activation (Fig. 6*B*). In addition, Ccd1 mutants D437A and ΔDIX that are unable to bind to Dvl failed to synergize with Dvl in stimulating Wnt signaling (Fig. 1*C*). Taken together, these data demonstrated that the tail of Ccd1-DIX interacts with Dvl, and that this heteromeric interaction is indispensable for Ccd1-medicated Wnt activate.

Given the head-to-tail model, the head of Dvl-DIX was, therefore, thought to be involved in the hetero-association with Ccd1-DIX, and we carried out pulldown assays with Dvl2-DIX mutants (Fig. 6*C*). Mutant Y27D at Site I of Dvl2-DIX ablated the hetero-interaction by disrupting the hydrophobic interaction, and substitutions of Ile-17 and Arg-84 with alanine in Dvl2-DIX that might weaken the interactions at Site II also led to severe compromise in the formation of hetero-complex. These critical residues are indeed clustered

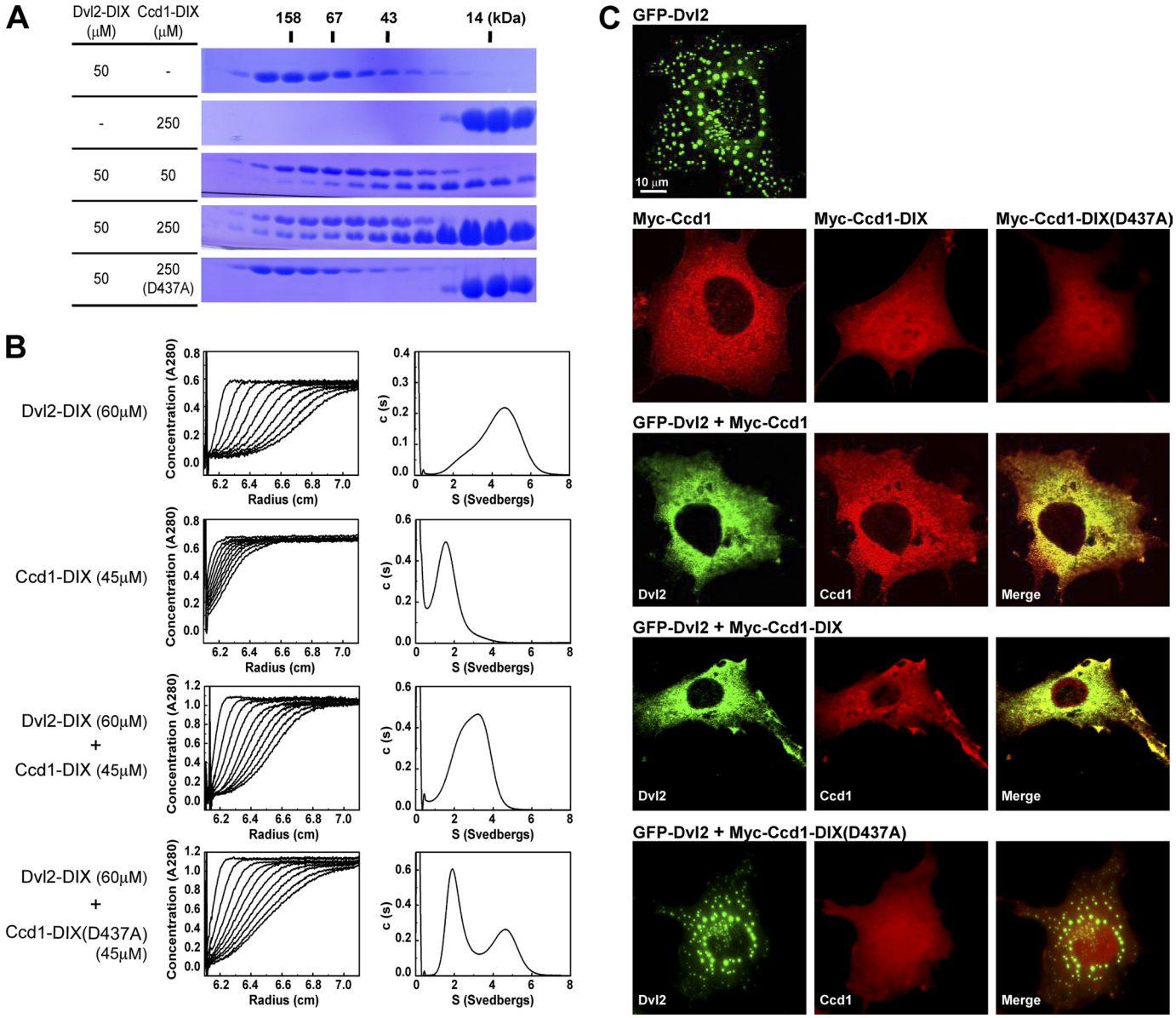

FIGURE 7. **Ccd1 depolymerizes Dvl homo-oligomer.** *A*, Ccd1-DIX converts the homo-assembly of Dvl2-DIX to a lower order. Dvl2-DIX was incubated with different amounts of Ccd1-DIX (wild type or mutant D437A), and the mixtures were subjected to gel filtration analysis. *B*, velocity ultracentrifugation analyses of Dvl2-DIX, Ccd1-DIX, and mixtures of Dvl2-DIX with Ccd1-DIX wild type or D437A mutant are shown. Shown on the *left* are the absorbance profiles at 280 nm as a function of radius at 15-min intervals, and the *right plots* are the distributions of sedimentation coefficients (*c*(*s*) *versus s*) calculated from the concentration profiles. *C*, effects of Ccd1 on the subcellular localizations of Dvl2 are shown. The *top four panels* show the localizations of Dvl2 and various Ccd1 proteins in individually transfected COS7 cells. The Dvl2 localization was visualized by the intrinsic fluorescence of GFP, whereas Ccd1 proteins were revealed by indirect immunofluorescence. COS7 cells were also co-transfected with 0.5 μg of GFP-Dvl2 and 0.5 μg of indicated Myc-Ccd1, and the co-localization signals appear *yellow* in merged pictures. *Scale bar*, 10 μm.

at the head of Dvl2-DIX. In addition, mutations at Site III that interfere with the interfilament interactions retained the ability to form hetero-complex with Ccd1 (data not shown). These data demonstrated that Dvl-DIX and Ccd1-DIX interact with each other through two distinct interfaces, the head of Dvl and the tail of Ccd1 (Fig. 6*D*).

Ccd1 Converts Polymeric Dvl to an Oligomer of Lower Order—In an attempt to analyze the interaction between Dvl-DIX and Ccd1-DIX using gel filtration assays, it was found that the addition of Ccd1-DIX converted the high molecular weight Dvl2-DIX polymer to complexes of lower order (Fig. 7*A*). Surprisingly, Dvl-DIX and Ccd1-DIX likely formed a 3:1 hetero-oligomer, but not a 1:1 heterodimer, even in the presence of 5-fold excess Ccd1-DIX. The Ccd1-DIX mutant D437A that is unable to bind to Dvl failed to attenuate the formation of Dvl2-DIX homopolymers regardless of the protein concentration. These data indicated that the hetero-interaction between Dvl-DIX and Ccd1-DIX is weaker than the homopolymerization of Dvl-DIX, which may result from the presence of a polar His side chain within the hydrophobic Site I of Ccd1-DIX (Fig. 3*B*). The depolymerization of Dvl by Ccd1 was confirmed by analytical ultracentrifugation (Fig. 7*B*). The sedimentation profile of the mixture of Dvl-DIX with wild type Ccd1-DIX was distinguished from those of the respective DIX proteins, and the calculated sedimentation value of the complex was approximate 3.2 S, lower than that of Dvl2-DIX ho-

mopolymer (~4.7 S). These data indicated that the Dvl2-Ccd1 complex exhibits an apparent molecular weight smaller than that of Dvl2 polymer. On the contrary, the mixture of Dvl-DIX with the non-interactive Ccd1-DIX(D437A) exhibited two separate peaks corresponding to the isolated proteins. Thus, wild type Ccd1 is able to depolymerize Dvl into lower order oligomers via the direct interactions between their DIX domains.

To explore the biological significance of this low molecular weight hetero-oligomer *in vivo*, we assessed the effect of Ccd1 on the puncta formation of Dvl (Fig. 7*C*). Coexpressing with wild type Ccd1 caused a dramatic change in Dvl2 localization; Dvl2 could no longer form puncta and became colocalized with Ccd1, evenly distributed throughout the cytoplasm. The same diffuse appearance was observed when Dvl2 was coexpressed with Ccd1-DIX alone, indicating that the DIX domain of Ccd1 is sufficient to disrupt the polymerization of Dvl *in vivo*. In contrast, coexpression of mutant Ccd1-DIX(D437A) that is defective in interacting with Dvl-DIX had little effect on the puncta formation of wild type Dvl2. These results suggested that Ccd1 is able to attenuate the homo-assembly of Dvl *in vitro* and induce a diffuse cytoplasmic distribution *in vivo*.

DISCUSSION

Although Ccd1 was shown to positively regulate the Wnt pathway (14, 36), the precise mechanism of Ccd1-mediated Wnt activation remains unsolved. We found that Ccd1 regulates Wnt signaling through the direct interaction with Dvl. Our study has further elucidated the structural basis for complex formations among the DIX domain proteins and demonstrated that the capability of Ccd1 to convert latent polymeric Dvl to biologically active oligomer underlies its positive role on Wnt signaling.

The structures of Ccd1-DIX and Dvl1-DIX(Y17D) belong to the ubiquitin-like fold, the same β-grasp topology as the previously determined Axin-DIX structure. Regardless of the distinct monomeric/oligomeric nature of the proteins used for structural studies, all three DIX domains form helical filaments in crystals, involving similar head-to-tail packing. It is noteworthy that a number of proteins form the head-to-tail complexes via association of their homotypic domains and, thus, exert widespread roles in the precise transduction of cellular signaling pathways (37–39). In addition to the previously identified hydrophobic interface (Site I), the crystal packing of Ccd1 and Dvl indicates additional contacts (Site II) between the N terminus of strand β1 or β5 of one molecule and the twisted β3-β4 loop of the adjacent molecule within the filament. Interestingly, the eight molecules of Dvl1-DIX(Y17D) within each asymmetric unit pack into two intertwined helical filaments, which enables us to identify a symmetric interfilament interface (Site III) for the assembly of higher order aggregate. Recently, some residues at Sites II and III were predicted to have potential roles in mediating DIX-DIX interaction by comparative modeling (40). Our structure-guided mutagenesis studies demonstrated that the integrity of the interface, including the primary Site I, the auxiliary Site II, and the interfilament Site III, is indispensable for Dvl homo-oligomerization, puncta formation, and Wnt signaling. In addition, Dvl and Ccd1 directly interact with each other through the head of Dvl-DIX and the tail of Ccd1-DIX, involving residues from Sites I and II. However, Axin-DIX may not possess an active Site II and is, therefore, incapable to form hetero-complex with Dvl-DIX and Ccd1-DIX (9, 11, 12, 26, 36). The hydrophobic pocket at Site II of Axin-DIX is partially deformed; a small Ala-756 on the head substitutes the bulky Leu/Ile in Ccd1/Dvl, and concomitantly the aromatic ring of Phe-801 on the tail of Axin shifts outwards more than 6 Å (Fig. 3*E*). Moreover, the charged residues forming salt bridges in Ccd1/Dvl are replaced by Ser-798 and Val-754 in Axin, which may lead to the disruption of the hydrophilic interactions at Site II. Therefore, Site II may be unique to Dvl-DIX and Ccd1-DIX.

Overexpressed Dvl has a tendency to form high molecular weight protein assemblies, visualized as puncta in cytosol, and the polymerization of Dvl is believed to be crucial for the initiation of Wnt signaling (5–9). Recently, the endogenous Dvl proteins were shown to display a diffuse or small punctate pattern in contrast to the heavy puncta of ectopically expressed Dvl (9, 41, 42). Bienz and co-workers (5, 8) have demonstrated that Dvl-DIX can undergo reversible polymerization/depolymerization and that endogenous Dvl2 forms far smaller oligomers, likely trimers. Importantly, the membrane-associated Dvl after Wnt stimulation appears to form smaller punctates than those in cytosol, suggesting that the large Dvl polymer undergoes a transient disassociation and subsequent translocation to the plasma membrane as low molecular weight oligomers (6, 7, 9, 43–45). Moreover, casein kinase Iϵ, a positive regulator of Wnt signaling, is able to bind to the PDZ and DEP domains of Dvl, phosphorylates it within a basic region, and induces a relatively even distribution within the cytoplasm in response to Wnt signal (46–48). Together, these results have indicated that the biologically active Dvl assemblies are in fact low molecular weight oligomers but not large punctate polymers as suggested by overexpression systems.

In the present study we observed that the positive Wnt regulator Ccd1, upon binding to Dvl, attenuates the homo-assembly of Dvl *in vitro* and leads to diffused cytoplasmic distribution of Dvl *in vivo*. Of a particular note, we have resolved a paradox between the observations that Dvl needs to homopolymerize for Wnt activation and that Ccd1 acts to depolymerize Dvl in Wnt activation. It is clear that a prior requirement for Dvl to exert its positive role in Wnt signaling is to be able to form a homo-assembly of at least a dimer, in fact, as aforementioned a trimer. In the resting state, Dvl proteins accumulate in cytosol and form large punctate polymers that may preclude the access of other Wnt components, including Axin, due to the tight self-association. The Dvl assemblies are dynamic, and Wnt stimulation triggers a membrane translocation of the low molecular weight Dvl oligomers by direct interaction with Frizzled receptors. Recently, the activation of Wnt signaling was found to coincide with the increase of Ccd1 protein level due to a decrease in its ubiquitin-mediated degradation (49). Thus, in response to Wnt stimulation, Ccd1 is somehow accumulated in cytosol, then recruited to the Dvl

polymer and concomitantly depolymerize it, yielding the biologically active trimer. Under this conjecture, Dvl, by virtue of this reversible homo-assembly, is able to both keep the Wnt activity in check and to stimulate Wnt signaling, depending on the availability of Wnt signal.

Acknowledgments—We thank Lu-Hua Lai for advice on ultracentrifugation analyses, and Jijie Chai and Maojun Yang for help on data collection and processing.

REFERENCES

1. Logan, C. Y., and Nusse, R. (2004) *Annu. Rev. Cell Dev. Biol.* **20,** 781–810
2. Clevers, H. (2006) *Cell* **127,** 469–480
3. Klaus, A., and Birchmeier, W. (2008) *Nat. Rev. Cancer* **8,** 387–398
4. Cadigan, K. M., and Nusse, R. (1997) *Genes Dev.* **11,** 3286–3305
5. Schwarz-Romond, T., Fiedler, M., Shibata, N., Butler, P. J., Kikuchi, A., Higuchi, Y., and Bienz, M. (2007) *Nat. Struct. Mol. Biol.* **14,** 484–492
6. Yang-Snyder, J., Miller, J. R., Brown, J. D., Lai, C. J., and Moon, R. T. (1996) *Curr. Biol.* **6,** 1302–1306
7. Axelrod, J. D., Miller, J. R., Shulman, J. M., Moon, R. T., and Perrimon, N. (1998) *Genes Dev.* **12,** 2610–2622
8. Schwarz-Romond, T., Merrifield, C., Nichols, B. J., and Bienz, M. (2005) *J. Cell Sci.* **118,** 5269–5277
9. Schwarz-Romond, T., Metcalfe, C., and Bienz, M. (2007) *J. Cell Sci.* **120,** 2402–2412
10. Sakanaka, C., and Williams, L. T. (1999) *J. Biol. Chem.* **274,** 14090–14093
11. Smalley, M. J., Sara, E., Paterson, H., Naylor, S., Cook, D., Jayatilake, H., Fryer, L. G., Hutchinson, L., Fry, M. J., and Dale, T. C. (1999) *EMBO J.* **18,** 2823–2835
12. Kishida, S., Yamamoto, H., Hino, S., Ikeda, S., Kishida, M., and Kikuchi, A. (1999) *Mol. Cell. Biol.* **19,** 4414–4422
13. Lu, Z., Liu, W., Huang, H., He, Y., Han, Y., Rui, Y., Wang, Y., Li, Q., Ruan, K., Ye, Z., Low, B. C., Meng, A., and Lin, S. C. (2008) *J. Biol. Chem.* **283,** 13132–13139
14. Shiomi, K., Uchida, H., Keino-Masu, K., and Masu, M. (2003) *Curr. Biol.* **13,** 73–77
15. Shiomi, K., Kanemoto, M., Keino-Masu, K., Yoshida, S., Soma, K., and Masu, M. (2005) *Brain Res. Mol. Brain Res.* **135,** 169–180
16. Soma, K., Shiomi, K., Keino-Masu, K., and Masu, M. (2006) *Gene Expr. Patterns* **6,** 325–330
17. Ikeuchi, Y., Stegmüller, J., Netherton, S., Huynh, M. A., Masu, M., Frank, D., Bonni, S., and Bonni, A. (2009) *J. Neurosci.* **29,** 4312–4321
18. Singh, K. K., Ge, X., Mao, Y., Drane, L., Meletis, K., Samuels, B. A., and Tsai, L. H. (2010) *Neuron* **67,** 33–48
19. Otwinowski, Z., and Minor, W. (1997) *Methods in Enzymology* (Carter, C. W., Jr., and Sweet, R. M., eds) Vol. 276, part A, pp. 307–326, Academic Press, New York
20. Schneider, T. R., and Sheldrick, G. M. (2002) *Acta Crystallogr. D Biol. Crystallogr.* **58,** 1772–1779
21. Murshudov, G. N., Vagin, A. A., and Dodson, E. J. (1997) *Acta Crystallogr. D Biol. Crystallogr.* **53,** 240–255
22. Emsley, P., and Cowtan, K. (2004) *Acta Crystallogr. D Biol. Crystallogr.* **60,** 2126–2132
23. McCoy, A. J., Grosse-Kunstleve, R. W., Adams, P. D., Winn, M. D., Storoni, L. C., and Read, R. J. (2007) *J. Appl. Crystallogr.* **40,** 658–674
24. Adams, P. D., Grosse-Kunstleve, R. W., Hung, L. W., Ioerger, T. R., McCoy, A. J., Moriarty, N. W., Read, R. J., Sacchettini, J. C., Sauter, N. K., and Terwilliger, T. C. (2002) *Acta Crystallogr. D Biol. Crystallogr.* **58,** 1948–1954
25. Schuck, P. (2000) *Biophys. J.* **78,** 1606–1619
26. Wong, C. K., Luo, W., Deng, Y., Zou, H., Ye, Z., and Lin, S. C. (2004) *J. Biol. Chem.* **279,** 39366–39373
27. Pan, W., Choi, S. C., Wang, H., Qin, Y., Volpicelli-Daley, L., Swan, L., Lucast, L., Khoo, C., Zhang, X., Li, L., Abrams, C. S., Sokol, S. Y., and Wu, D. (2008) *Science* **321,** 1350–1353
28. Korinek, V., Barker, N., Morin, P. J., van Wichen, D., de Weger, R., Kinzler, K. W., Vogelstein, B., and Clevers, H. (1997) *Science* **275,** 1784–1787
29. Greco, T. L., Sussman, D. J., and Camper, S. A. (1996) *Mamm. Genome* **7,** 475–476
30. Klingensmith, J., Yang, Y., Axelrod, J. D., Beier, D. R., Perrimon, N., and Sussman, D. J. (1996) *Mech. Dev.* **58,** 15–26
31. Pizzuti, A., Amati, F., Calabrese, G., Mari, A., Colosimo, A., Silani, V., Giardino, L., Ratti, A., Penso, D., Calzà, L., Palka, G., Scarlato, G., Novelli, G., and Dallapiccola, B. (1996) *Hum. Mol. Genet.* **5,** 953–958
32. Sussman, D. J., Klingensmith, J., Salinas, P., Adams, P. S., Nusse, R., and Perrimon, N. (1994) *Dev. Biol.* **166,** 73–86
33. Tsang, M., Lijam, N., Yang, Y., Beier, D. R., Wynshaw-Boris, A., and Sussman, D. J. (1996) *Dev. Dyn.* **207,** 253–262
34. Wallingford, J. B., and Habas, R. (2005) *Development* **132,** 4421–4436
35. Lee, Y. N., Gao, Y., and Wang, H. Y. (2008) *Cell. Signal.* **20,** 443–452
36. Luo, W., Zou, H., Jin, L., Lin, S., Li, Q., Ye, Z., Rui, H., and Lin, S. C. (2005) *J. Biol. Chem.* **280,** 5054–5060
37. Park, H. H., Lo, Y. C., Lin, S. C., Wang, L., Yang, J. K., and Wu, H. (2007) *Annu. Rev. Immunol.* **25,** 561–586
38. Qiao, F., Song, H., Kim, C. A., Sawaya, M. R., Hunter, J. B., Gingery, M., Rebay, I., Courey, A. J., and Bowie, J. U. (2004) *Cell* **118,** 163–173
39. Sumimoto, H., Kamakura, S., and Ito, T. (2007) *Sci STKE* **2007,** re6
40. Ehebauer, M. T., and Arias, A. M. (2009) *BMC Struct. Biol.* **9,** 70
41. Bilic, J., Huang, Y. L., Davidson, G., Zimmermann, T., Cruciat, C. M., Bienz, M., and Niehrs, C. (2007) *Science* **316,** 1619–1622
42. Smalley, M. J., Signoret, N., Robertson, D., Tilley, A., Hann, A., Ewan, K., Ding, Y., Paterson, H., and Dale, T. C. (2005) *J. Cell Sci.* **118,** 5279–5289
43. Miller, J. R., Rowning, B. A., Larabell, C. A., Yang-Snyder, J. A., Bates, R. L., and Moon, R. T. (1999) *J. Cell Biol.* **146,** 427–437
44. Rothbächer, U., Laurent, M. N., Deardorff, M. A., Klein, P. S., Cho, K. W., and Fraser, S. E. (2000) *EMBO J.* **19,** 1010–1022
45. Cong, F., Schweizer, L., and Varmus, H. (2004) *Development* **131,** 5103–5115
46. Peters, J. M., McKay, R. M., McKay, J. P., and Graff, J. M. (1999) *Nature* **401,** 345–350
47. Kishida, M., Hino, Si., Michiue, T., Yamamoto, H., Kishida, S., Fukui, A., Asashima, M., and Kikuchi, A. (2001) *J. Biol. Chem.* **276,** 33147–33155
48. Cong, F., Schweizer, L., and Varmus, H. (2004) *Mol. Cell. Biol.* **24,** 2000–2011
49. Wang, L., Li, H., Chen, Q., Zhu, T., Zhu, H., and Zheng, L. (2010) *Cancer Sci.* **101,** 700–706